

# Robust Low-light Scene Restoration via Illumination Transition

Ze Li<sup>1,2</sup> Feng Zhang<sup>3,2</sup> Xiatian Zhu<sup>4</sup> Meng Zhang<sup>1,2</sup> Yanghong Zhou<sup>2</sup> P. Y. Mok<sup>1\*</sup>

<sup>1</sup>The Hong Kong University of Science and Technology, Hong Kong SAR

<sup>2</sup>The Hong Kong Polytechnic University, Hong Kong SAR

<sup>3</sup>Nanjing University of Posts and Telecommunications, Nanjing, China

<sup>4</sup>University of Surrey, Guildford, United Kingdom

## Abstract

Synthesizing normal-light novel views from low-light multiview images is an important yet challenging task, given the low visibility and high ISO noise present in the input images. Existing low-light enhancement methods often struggle to effectively preprocess such low-light inputs, as they fail to consider correlations among multiple views. Although other state-of-the-art methods have introduced illumination-related components offering alternative solutions to the problem, they often result in drawbacks such as color distortions and artifacts, and they provide limited denoising effectiveness. In this paper, we propose a novel **Robust Low-light Scene Restoration** framework (**RoSe**), which enables effective synthesis of novel views in normal lighting conditions from low-light multiview image inputs, by formulating the task as an illumination transition estimation problem in 3D space, conceptualizing it as a specialized rendering task. This multiview-consistent illuminance transition field establishes a robust connection between low-light and normal-light conditions. By further exploiting the inherent low-rank property of illumination to constrain the transition representation, we achieve more effective denoising without complex 2D techniques or explicit noise modeling. To implement RoSe, we design a concise dual-branch architecture and introduce a low-rank denoising module. Experiments demonstrate that RoSe significantly outperforms state-of-the-art models in both rendering quality and multiview consistency on standard benchmarks. The codes and data are available at <https://pegasus2004.github.io/RoSe>.

## 1. Introduction

The synthesis of a normal-light 3D scene from low-light multiview images [5, 34] remains a valuable yet challenging task, as in many real-world applications where well-lit

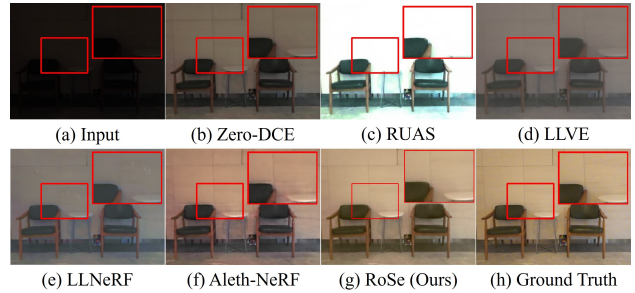


Figure 1. Image/video enhancement (Zero-DCE [8]+NeRF, RUAS [15]+NeRF, LLVE [43]+NeRF) vs. state-of-the-art models (LLNeRF [34], Aleth-NeRF [5]) vs. our RoSe.

data acquisition is often not feasible. Recent advancements in techniques such as Neural Radiance Fields (NeRFs) [19] have demonstrated impressive capabilities in 3D scene representation; however, they struggle in low-light conditions because of the reliance on direct color optimization, which becomes unreliable in cases of low visibility or high ISO noise.

Existing low-light enhancement methods [4, 8, 15, 17, 43] offer a straightforward solution by converting low-light inputs into normal-light images either before or after 3D scene optimization. However, these methods often result in low-quality novel view images with artifacts and color distortion (Fig. 1(b-d)), as these enhancement methods primarily focus on improving individual views independently without considering the multiview relationship.

More recently, new approaches are proposed. For example, LLNeRF [34] improves brightness by learning per-view enhancement coefficients for the view-dependent color component of 3D sampling points. However, since the view-dependent components decoupled from the same sampling point vary across different viewpoints, LLNeRF may introduce conflicting enhancements for that point, leading to artifacts and color distortion in the synthesized images (Fig. 1(e)). Aleth-NeRF [5] proposes a counter intuitive yet effective approach by assigning non-zero transmittance val-

\*Corresponding author: tracy.mok@ust.hk

ues to air particles to model light attenuation. However, this makes air behave more like a light-absorbing medium such as fog or water. When there is a large brightness gap between the low-light observations and the target restored scene, high opacity values may cause the network to misinterpret air as part of the objects and lead to color distortion (Fig. 1(f) and Fig. 4). Moreover, both methods rely solely on NeRF’s multiview optimization for implicit denoising. If noise remains consistent across views, they may misinterpret such noise as part of the scene geometry, leading to artifacts.

In this work, we present **RoSe**, a **robust low-light scene restoration framework** for synthetic normal-light novel views from noisy, low-light multiview inputs. Inspired by 2D Retinex theory [23], we frame this task as an illuminance transition estimation problem in 3D space and conceptualize it as a specialized rendering task. Specifically, RoSe employs a dual-branch architecture consisting of two key components: a viewer-centered normal-light scene representation that captures the light interactions between objects and viewers, and a world-centered illuminance transition estimation that learns multiview-consistent transformations from low-light to normal-light settings. The two branches work together to represent the observed low-light scenes, establishing a robust connection between low-light and normal-light conditions.

This design is further enhanced by leveraging the inherent low-rank nature of illumination, which contrasts with the high-rank randomness of noise. To this end, a low-rank denoising module (LRD) is integrated into the illuminance transition estimation branch to eliminate artifacts and improve the structural integrity of the scene. As shown in Fig. 1(g), RoSe can render clear, normal-light novel views from low-light inputs, outperforming the state-of-the-art methods [5, 34] and other light-enhancement based methods [4, 8, 15].

Our contributions are as follows:

- We reformulate the low-light scene restoration task as an illuminance transition estimation problem.
- We further conceptualize this illuminance transition estimation process as a specialized rendering problem, leveraging the low-rank property of illumination for effective denoising.
- We propose RoSe a novel architecture with a robust unsupervised illumination-aware restoration for this task.
- Experiments show that RoSe achieves superior visual quality and multiview consistency compared to state-of-the-art alternatives.

## 2. Related Work

### 2.1. Neural Radiance Field

Neural Radiance Fields [19] represent continuous 3D scenes by predicting density and color information for each point in 3D space, enabling high-quality novel view synthesis. While recent advances have addressed various limitations of NeRF, such as dense view requirements [10, 22, 30, 42] and long training times [6, 7, 24], significant challenges remain in handling adverse lighting conditions. Many studies have aimed to improve NeRF’s robustness in adverse lighting environments, such as images with unconstrained exposure [12, 18, 25, 27, 46], relighting [26, 32, 38], and underwater scenes [31, 45]. However, low-light scene restoration presents unique challenges for NeRF due to low visibility and high ISO noise, making accurate geometry inference difficult.

For 3D scenes with low-light inputs, RAW-NeRF [20] renders NeRF directly on noisy raw HDR images, enhanced with an image signal processor (ISP). However, the requirement of HDR RAW data for training makes it hard to generalize on commonly used sRGB images. LLNeRF [34] utilizes NeRF’s multiview optimization for denoising. It also proposes to decompose and manipulate illumination components along viewing rays to enhance the brightness. However, the view-dependent decomposition suffers from inconsistent illumination factorization across different viewpoints due to varying ray sampling distributions, leading to unstable rendering results. Aleth-NeRF [5] introduced concealing fields that model light attenuation from normal-light to low-light scenes by assigning non-zero transmittance values to air particles. By removing the learned concealing fields, Aleth-NeRF can achieve effective scene illumination restoration. However, when there is a significant illumination gap between low-light observation and normal-light scenes, Aleth-NeRF assigns high opacity to air particles, leading to the network misjudging them as part of the object.

In this work, we reformulate the task as an illuminance transition estimation problem. By modeling illuminance transition as a specialized neural field, we establish a physically consistent mapping between low-light and normal-light scene representations, enabling robust novel view synthesis while preserving scene structure.

### 2.2. Low-light Enhancement

In recent years, advances in deep learning have markedly improved low-light image enhancement (LIE) performance. Many existing methods [28, 36, 37, 39, 40] rely on paired training data for brightness enhancement, yet capturing paired low-light and normal-light images in real-world settings is impractical. To address this, unsupervised GAN-based approaches, such as EnlightenGAN [11], eliminate

the need for paired data but require careful curation of unpaired data. Alternatively, zero-reference methods [8, 14, 15, 17, 47] avoid using ground-truth supervision altogether, relying on encoded priors to guide enhancement.

The Retinex theory [23] provides a fundamental framework for low-light enhancement by mathematically relating low-light observations to normal-light images, which has inspired many effective solutions. For instance, Liu et al. [15] use Retinex principles to develop an enhancement model that unrolls illumination estimation and noise removal steps within an optimization framework, augmented by learnable architecture search. Similarly, Ma et al. [17] propose a Self-Calibrated Illumination (SCI) learning framework based on Retinex theory, where a self-calibration module estimates reflectance, iteratively refining illumination maps to produce enhanced outputs after illumination is removed.

Despite these advances, existing methods predominantly operate in 2D image space, failing to leverage the inherent 3D geometry of scenes or accommodate multi-view inputs effectively. While video enhancement methods [16, 43] have made progress in maintaining temporal consistency between adjacent frames, they primarily focus on enhancing original viewpoints rather than generating coherent 3D scenes with novel views.

Unlike traditional Retinex-based methods confined to 2D applications, we explicitly model an illuminance transition field to bridge the normal-light scene representation and the low-light observed scene. This illuminance transition field represents a fundamental shift in how illumination is handled in multiview scenarios, enabling coherent illuminance transition across different viewpoints while preserving scene structure.

### 3. Robust Low-light Scene Restoration

#### 3.1. Motivation

In Retinex theory [23], an image  $Z \in \mathbf{R}^{H \times W \times 3}$  can be represented as reflectance  $R \in \mathbf{R}^{H \times W \times 3}$  and illumination  $L \in \mathbf{R}^{H \times W \times 1}$  as follows:

$$Z = R \odot L, \quad (1)$$

where  $\odot$  denotes element-wise multiplication. Many Retinex-based methods [2, 15, 17, 35, 36, 41] adopt a decomposition-and-enhancement pipeline to restore the normal-light image  $Z_{nor}$  from the low-light observations  $Z_{low}$ . However, the decomposition is ill-posed, requiring additional constraints on both  $R$  and  $L$ . Since the illumination can not be thoroughly decomposed, the enhancement process may result in color distortion, requiring ground truth data for supervision.

To address these limitations, we introduce an illuminance transition component  $I \in \mathbf{R}^{H \times W \times 1}$  to establish a

direct connection between  $Z_{nor}$  and  $Z_{low}$ , thereby reformulating low-light scene restoration as an illuminance transition estimation problem. According to the Retinex theory [23], reflectance  $R$  is an invariant intrinsic property of a scene, i.e.,  $R_{nor} = R_{low}$ . Given  $Z_{nor} = R_{nor} \odot L_{nor}$  and  $Z_{low} = R_{low} \odot L_{low}$ , this leads to the following formulation:

$$Z_{low} = Z_{nor} \odot I, \quad (2)$$

where  $I = \frac{L_{low}}{L_{nor}}$ . This simplified formulation enables direct recovery of normal-light image  $Z_{nor}$  from low-light input  $Z_{low}$  by estimating the illuminance transition  $I$ , bypassing the need for two-stage decomposition and enhancement. As  $I$  encodes the relative illumination ratio  $\frac{L_{low}}{L_{nor}}$  rather than directly modulating illumination  $L$  or reflectance  $R$ , it inherently preserves the scene’s color properties, mitigating the potential color deviation issue. Building on this insight, we extend this formulation to 3D space, introducing **RoSe**, a robust low-light scene restoration framework.

#### 3.2. Architecture

In 3D space, we treat each pixel in the image  $Z$  and the illuminance transition component  $I$  as the result of a volume rendering process, where the accumulated radiance and illuminance transition value along each camera ray yield the observed color  $\hat{C}$  and illuminance component  $\hat{I}$ , respectively. Based on this view, we conceptualize illuminance transition estimation as a specialized rendering problem, resulting in a concise dual-branch architecture.

As shown in Fig. 2 (a), RoSe takes 3D location  $\mathbf{x}$  and view direction  $\mathbf{d}$  as input to jointly model the normal-light scene representation  $(\mathbf{c}, \sigma)$  and the illuminance transition field  $(i, \sigma)$ . The normal-light scene learning is viewer-centered, capturing the lighting effects between the observer and the object. The illuminance transition learning is world-centered, ensuring consistent illuminance transitions across different viewpoints. Through volume rendering, it generates normal-light RGB value  $\hat{C}_{nor}$  and illuminance transition value  $\hat{I}$ , which together reconstruct the observed low-light pixels  $\hat{C}_{low}$ :

$$\hat{C}_{low} = \hat{C}_{nor} \odot \hat{I}. \quad (3)$$

Since noise is a 2D phenomenon caused by the imaging sensor, we neither model it explicitly in 3D space nor rely on additional 2D denoising techniques. Instead, we leverage the low-rank property of illumination for noise suppression and introduce a low-rank denoising (LRD) module within our illuminance transition branch (Fig. 2 (b)).

The network is trained using only low-light observed images as supervision through a mean square error loss. Additionally, an unsupervised illumination correction loss ensures that the normal-light scene recovers to the target illumination level. The following sections will detail the core components of our framework.

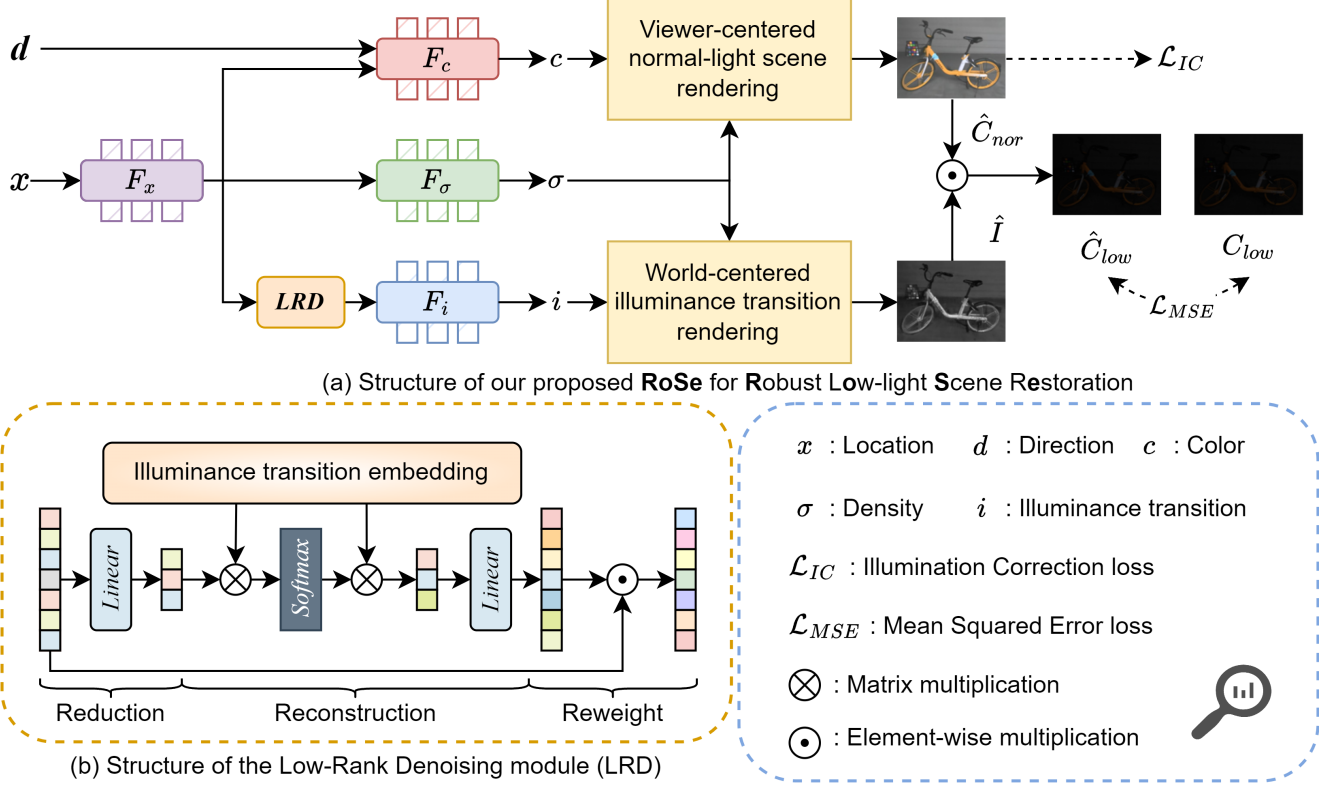


Figure 2. An overview of the proposed RoSe framework. It learns both normal-light scene representation ( $\mathbf{c}, \sigma$ ) and illuminance transition ( $i, \sigma$ ) from the low-light scene. A low-rank denoising module (LRD) is integrated into the illuminance transition estimation branch, leveraging the low-rank property of illumination for denoising. Through volume rendering (Eq. (6), Eq. (8)), it generates illuminance transition value  $\hat{I}$  and normal-light RGB values  $\hat{C}_{nor}$ , which combine to represent observed low-light pixels  $\hat{C}_{low}$  (Eq. (3)). The network is trained using only low-light observed images as supervision through a mean square error loss as used in NeRF, complemented by an unsupervised illumination correction loss.

**Viewer-centered normal-light scene rendering.** The normal-light scene representation branch follows the standard NeRF formulation:

$$F(\mathbf{x}, \mathbf{d}) \rightarrow (\mathbf{c}, \sigma), \quad (4)$$

where  $\mathbf{x} = (x, y, z)$  denotes the 3D spatial coordinates of sample points along a camera ray, and  $\mathbf{d} = (\theta, \phi)$  represents the viewing direction.  $\mathbf{c} = (r, g, b)$  and  $\sigma$  are predicted color and volume density of each sample point. This formulation captures the interaction of light with the scene geometry from a location to the viewer, making it inherently viewer-centered.

For the network structure, we adopt three multilayer perceptrons (MLPs): a location MLP  $F_x$ , a density MLP  $F_\sigma$ , and a color MLP  $F_c$ . These MLPs map the 3D spatial coordinates  $\mathbf{x}$  and viewing direction  $\mathbf{d}$  to the corresponding density  $\sigma$  and color  $\mathbf{c}$ :

$$\sigma = F_\sigma(F_x(\mathbf{x})), \mathbf{c} = F_c(F_x(\mathbf{x}), \mathbf{d}). \quad (5)$$

The predicted color and density values of all sample points

along a camera ray  $\mathbf{r}$  are then integrated to render the expected color  $\hat{C}_{nor}(\mathbf{r})$ . In practice, the integrals are approximated through discrete computation:

$$\hat{C}_{nor}(\mathbf{r}) = \sum_{n=1}^N T_n (1 - \exp(-\sigma_n \delta_n)) \mathbf{c}_n, \quad (6)$$

where  $T_n = \exp\left(-\sum_{j=1}^{n-1} \sigma_j \delta_j\right)$ ,  $N$  is the total number of sample points and  $\delta_n = t_{n+1} - t_n$  is the distance between adjacent samples.

**World-centered illuminance transition rendering.** As normal-light scene representation already captures view-dependent effects, we argue that the illuminance transition should be world-centered. When the illuminance transition field remains consistent across different viewpoints, it ensures stable illumination transitions and effectively avoids artifacts.

To achieve this, we introduce a world-centered illuminance transition estimation branch. This branch includes an illuminance transition MLP  $F_i$  for estimating  $i$ , which is

solely dependent on the 3D spatial location:

$$i = F_i(F_x(x)). \quad (7)$$

Similar to the normal-light scene rendering, we use a discrete approximation to estimate the integral of the predicted illuminance transition value  $i$  and obtain the illuminance transition value  $\hat{I}(\mathbf{r})$  along a camera ray:

$$\hat{I}(\mathbf{r}) = \sum_{n=1}^N T_n (1 - \exp(-\sigma_n \delta_n)) i_n, \quad (8)$$

where  $T_n = \exp\left(-\sum_{j=1}^{n-1} \sigma_j \delta_j\right)$ ,  $N$  is the total number of sample points and  $\delta_n = t_{n+1} - t_n$  is the distance between adjacent samples.

**Low-rank denoising.** The spatial smoothness of illumination inherently reflects its low-rank nature, while noise is typically random and high-rank. Thus, effective denoising can be achieved by simply constraining this property, without relying on 2D denoising techniques or explicit noise modeling.

As shown in Fig. 2 (b), our low-rank denoising module follows a reduction-reconstruction-reweight process to implement low-rank regularization. In the first stage, the input feature  $f_x \in \mathbb{R}^{B \times C}$  is projected into a low-rank subspace via a linear transformation, producing  $f_k \in \mathbb{R}^{B \times k}$ :

$$f_k = \text{Linear}(f_x), \quad (9)$$

After that, a set of learnable low-rank filters is introduced as the illuminance transition embedding  $E \in \mathbb{R}^{k \times M}$ . Inspired by the attention mechanism [33], we then calculate the similarity between  $f_k$  and  $E$  to reconstruct the most relevant low-rank feature  $f_g \in \mathbb{R}^{B \times k}$ :

$$w = \text{Softmax}(f_k \otimes E), f_g = w \otimes E, \quad (10)$$

where  $\otimes$  denotes matrix multiplication.

Rather than directly replacing the original feature,  $f_g$  serves as a guidance signal. This avoids the limitations of low-rank representations, which may lose spatial details. The reconstructed feature is expanded back to the original dimensionality and used to reweight the input:

$$f'_g = \text{Linear}(f_g), f'_i = f'_g \odot f_x. \quad (11)$$

By doing so, we can suppress high-rank noise, thereby improving object geometry estimation.

### 3.3. Optimization

During training, the normal-light scene representation is optimized unsupervisedly. Specifically, an illumination correction loss is used to regulate the global illumination level, while a reconstruction loss between low-light observations

and reconstructed images is applied to learn the underlying scene geometry. Details are provided below.

**Illumination correction loss.** We introduce a hyperparameter  $e$  to represent the desired illumination level for the normal-light scene and apply an unsupervised illumination correction loss  $\mathcal{L}_{IC}$  to the rendered normal-light image, regulating it by minimizing the difference between the average intensity of the rendered image and the desired illumination level  $e$ :

$$\mathcal{L}_{IC} = \left\| \text{GAP}(\hat{C}_{nor}(\mathbf{r})) - e \right\|^2, \quad (12)$$

where  $\text{GAP}(\cdot)$  denotes global average pooling. In our experiments, we set  $e$  to 0.45 to achieve balanced performance.

**NeRF regression loss.** As dark pixels with small values would contribute minimally, while bright pixels with larger values would dominate the contribution. We apply an inverse tone curve [1] to rebalance pixel weights before computing the MSE loss:

$$\begin{aligned} \phi(x) &= \frac{1}{2} - \sin\left(\frac{\sin^{-1}(1-2x)}{3}\right), \\ \mathcal{L}_{\text{MSE}} &= \sum_r^R \left\| \hat{C}_{low}(\mathbf{r}) - \phi(C_{low}(\mathbf{r}) + \varepsilon) \right\|^2, \end{aligned} \quad (13)$$

where  $\varepsilon = 1e - 3$ , and  $R$  is the total number of pixels in the reconstructed image. Notably, while the inverse tone curve rebalances pixel weights, it also amplifies noise, which necessitates dedicated denoising.

As a result, the overall loss function for RetinexLight is defined as follows:

$$\mathcal{L} = \mathcal{L}_{\text{MSE}} + \lambda \mathcal{L}_{IC}, \quad (14)$$

where  $\lambda$  is set to  $1e^{-3}$ .

## 4. Experiments

**Dataset.** We conducted all experiments on the LOM dataset [5], which contains five scenes with 25–48 images captured under different exposure settings to simulate low-light and normal-light conditions. For dataset split, we used 3–5 images for testing, 1 image for validation, and the rest for training in each scene.

**Implementation details.** During training, we used the Adam optimizer with an initial learning rate of  $5e - 4$  and cosine learning rate decay every 2500 iterations. The training batch size was 1024, and the total number of iterations was 75000. We employed hierarchical sampling with 64 coarse and 128 fine samples per ray, as in NeRF [19]. For fair comparisons, all methods were retrained on the LOM dataset using their default optimal settings.

Table 1. The quantitative comparison results between ours and existing methods on test scenes with paired normal-light images. Metrics: PSNR(P) $\uparrow$ , SSIM(S) $\uparrow$ , and LPIPS(L) $\downarrow$ . **Bold**: The best result; underline: The second best result.

Method	“buu”	“chair”	“sofa”	“bike”	“shrub”	mean
	PSNR/SSIM/LPIPS	PSNR/SSIM/LPIPS	PSNR/SSIM/LPIPS	PSNR/SSIM/LPIPS	PSNR/SSIM/LPIPS	PSNR/SSIM/LPIPS
NeRF [19]	7.51/0.291/0.448	6.04/0.147/0.594	6.28/0.210/0.568	6.35/0.072/0.623	8.03/0.201/0.680	6.84/0.150/0.582
Image enhancement methods						
LIME [9]	13.92/0.795/0.302	11.33/0.698/0.509	12.26/0.759/0.444	11.26/0.589/0.439	14.16/0.424/0.465	12.59/0.653/0.432
DUAL [44]	13.11/0.770/0.305	10.36/0.651/0.500	11.20/0.713/0.429	9.24/0.433/0.470	13.97/0.415/0.470	11.58/0.596/0.435
RetinexNet [35]	16.19/0.780/0.396	16.89/0.756/0.543	16.98/0.807/0.577	18.00/0.707/0.482	14.86/0.284/0.518	16.58/0.667/0.503
Zero-DCE [8]	17.90/0.858/0.376	12.58/0.721/0.460	14.45/0.831/0.419	10.39/0.518/0.464	12.32/0.308/0.481	13.53/0.649/0.432
SCI [17]	7.76/0.692/0.525	19.77/0.802/0.674	10.08/0.772/0.520	13.44/0.658/0.435	18.16/0.503/0.475	13.84/0.689/0.510
IAT [4]	14.46/0.705/0.386	18.70/0.780/0.665	17.88/0.829/0.547	13.65/0.616/0.528	13.87/0.317/0.536	15.71/0.649/0.532
RUAS [15]	17.89/0.869/0.336	12.59/0.721/0.459	17.05/0.808/0.575	10.39/0.519/0.463	12.33/0.308/0.479	14.05/0.645/0.462
Retinexformer [2]	<u>24.90/0.891/0.308</u>	20.30/0.821/0.581	19.10/0.868/0.432	13.57/0.659/0.454	16.61/0.412/0.539	21.71/0.730/0.463
Video enhancement methods						
MBLLEN [16]	22.39/0.877/0.353	23.59/0.788/0.559	19.99/0.836/0.542	14.09/0.636/0.525	13.17/0.501/0.555	18.65/0.728/0.507
LLVE [43]	19.97/0.848/0.393	15.17/0.764/0.610	18.17/0.855/0.465	13.84/0.638/0.492	15.35/0.287/0.577	16.50/0.678/0.507
End-to-end enhancement methods						
LLNeRF [34]	24.05/0.849/0.351	<u>27.06/0.863/0.400</u>	<u>26.17/0.878/0.416</u>	20.17/ <b>0.788/0.358</b>	18.22/ <b>0.643/0.384</b>	<u>23.13/0.804/0.382</u>
Aleth-NeRF [5]	20.22/0.859/0.315	20.93/0.818/0.468	19.52/0.857/0.354	<u>20.46/0.727/0.499</u>	<u>18.24/0.511/0.448</u>	19.87/0.754/0.417
RoSe	<b>30.03/0.918/0.274</b>	<b>29.27/0.879/0.345</b>	<b>30.00/0.900/0.380</b>	<u>23.82/0.782/0.451</u>	<u>18.26/0.561/0.439</u>	<b>26.28/0.808/0.379</b>

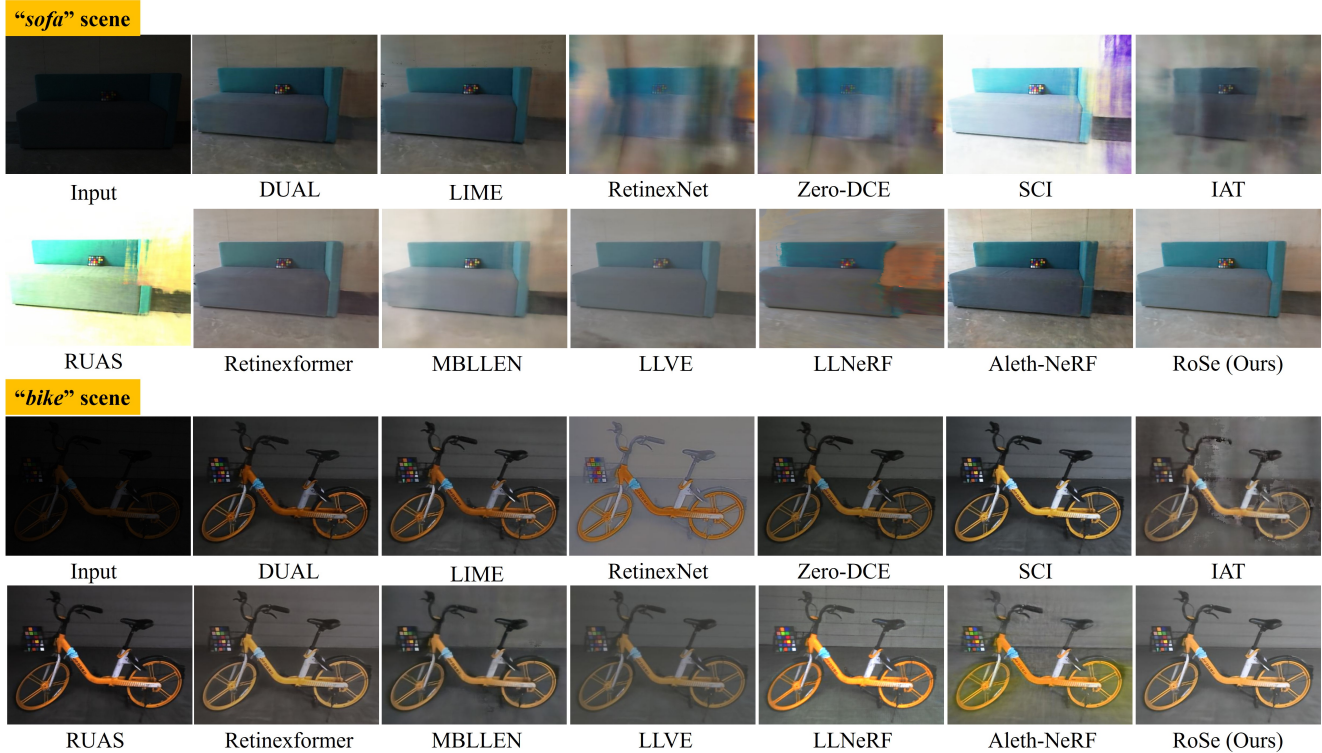


Figure 3. Normal-light novel view synthesis comparison in low-light conditions.

## 4.1. Main Results

**Quantitative comparison.** We quantitatively compared RoSe with state-of-the-art low-light enhancement and end-to-end methods using PSNR, SSIM, and LPIPS metrics across five scenes. As a baseline, we first trained a vanilla

NeRF under low-light conditions (Table 1, first row).

We then applied several traditional and advanced low-light enhancement methods to preprocess images before NeRF training, not but for postprocessing, as prior studies [5] showed that postprocessing generally underperforms

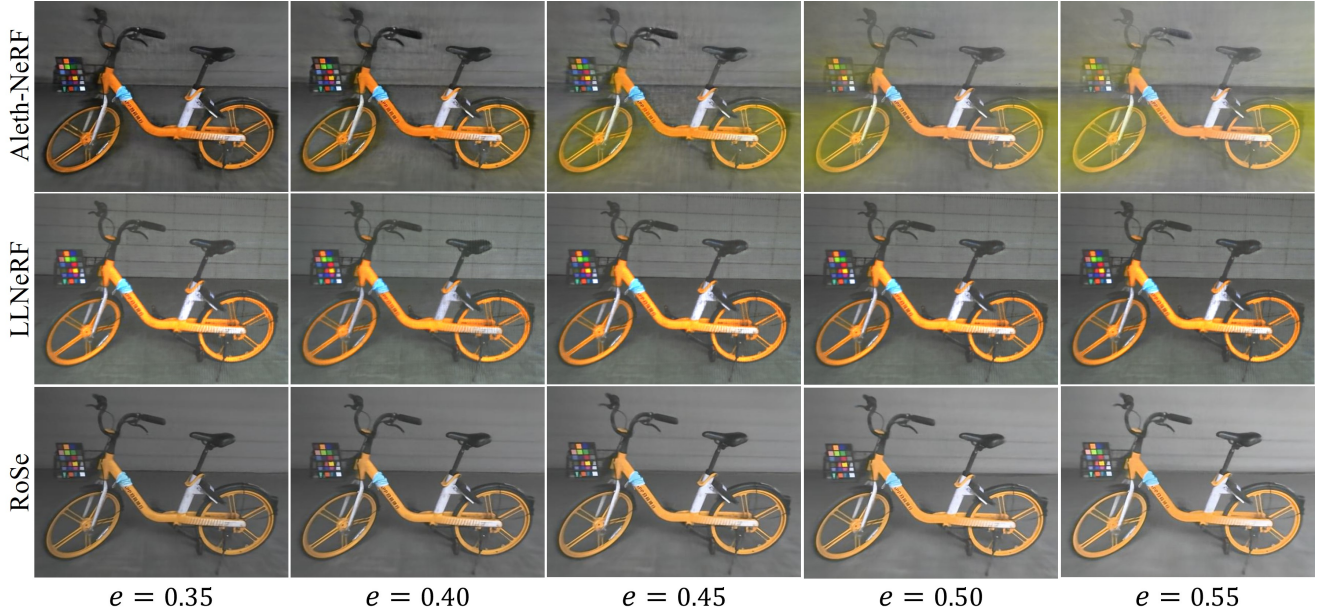


Figure 4. Ablation study on the effect of illumination level  $e$  in illumination correction loss. RoSe achieves robust illumination recovery across varying illumination levels without artifacts or color distortion.

compared to preprocessing. We also compared RoSe with advanced end-to-end methods, LLNeRF and Aleth-NeRF.

As shown in Table 1, traditional methods [9, 44] performed poorly due to noise amplification during enhancement. Learning-based methods [2, 4, 8, 15–17, 35, 43] also failed to improve significantly due to color and structural distortions from multiview inconsistencies. Overall, end-to-end methods [5, 34] outperformed enhancement-based approaches, with our method achieving the best or second-best performance across all five scenes.

**Qualitative comparison.** Figure 3 presents qualitative visualizations of the "sofa" and "bicycle" scenes from the LOM dataset. It is evident that low-light enhancement methods fail to recover reasonable scene brightness and structure when integrated with NeRF due to their view-inconsistent enhancement. Current state-of-the-art end-to-end models also show limitations: LLNeRF exhibits noticeable artifacts in both scenes due to conflicts introduced by its viewpoint-dependent enhancement. Aleth-NeRF suffers from color distortions due to alterations in the properties of air particles. In comparison, RoSe generates more stable and vivid novel view images while better preserving the scene structure.

## 4.2. Ablation Study

**Effect of illumination level in  $\mathcal{L}_{IC}$ .** The illumination level of the reconstructed target scene should not be fixed, as the precise level is unknown. We conducted ablation studies on the hyperparameter  $e$  for illumination correction, compar-

ing it to analogous parameters in Aleth-NeRF and LLNeRF. As shown in Figure 4, Aleth-NeRF is highly sensitive to hyperparameter adjustments, leading to color distortions and diffusion artifacts. This instability stems from its method of modeling light attenuation by assigning transmittance values to air particles. When there is a large illumination gap, Aleth-NeRF misinterprets air as scene geometry. LLNeRF, on the other hand, lacks controllable illumination adjustment due to its view-inconsistent enhancement, which also results in artifacts. In contrast, RoSe demonstrates stable illumination adjustment capabilities across various hyperparameter settings without compromising structural integrity.

**Order of LRD and illuminance transition MLP  $F_i$ .** We conducted ablation studies on the ordering of the low-rank denoising module (LRD) and illuminance transition MLP  $F_i$  to identify the optimal position of LRD. Specifically, we compared two configurations: LRD-first and MLP-first. As shown in Table 2, while both configurations yield comparable performance, LRD-first performs better on PSNR, SSIM, and LPIPS metrics. We therefore adopt the LRD-first configuration in our final model.

**Effect of low-rank denoising.** The smoothness of illumination implies a low-rank structure, which we leverage via a low-rank denoising (LRD) module. To validate its denoising effect, we compare four settings: (1) without LRD (w/o LRD), (2) with total variation (TV) loss [13] (w/ TV) as an alternative, (3) with LRD (w/ LRD), and (4) LRD combined with TV loss (LRD+TV).

As shown in Figure 5, without LRD, noise causes in-

Table 2. Ablation study on the order of low-rank denoising module (LRD) and illuminance transition MLP  $F_i$ .

Method	“buu”	“chair”	“sofa”	“bike”	“shrub”	mean
	PSNR/SSIM/LPIPS	PSNR/SSIM/LPIPS	PSNR/SSIM/LPIPS	PSNR/SSIM/LPIPS	PSNR/SSIM/LPIPS	PSNR/SSIM/LPIPS
MLP-first	30.00/0.919/0.273	29.21/0.849/0.350	30.07/0.899/0.381	23.93/0.781/0.449	17.95/0.518/0.478	26.23/0.793/0.386
LRD-first	30.03/0.918/0.274	29.27/0.879/0.345	30.00/0.900/0.380	23.82/0.782/0.451	18.26/0.561/0.439	26.28/0.808/0.379

Table 3. Ablation study on the low-rank denoising (LRD) module. “w/o” and “w/” denote the absence and presence, respectively. “TV” refers to total variation loss [13].

Method	“buu”	“chair”	“sofa”	“bike”	“shrub”	mean
	PSNR/SSIM/LPIPS	PSNR/SSIM/LPIPS	PSNR/SSIM/LPIPS	PSNR/SSIM/LPIPS	PSNR/SSIM/LPIPS	PSNR/SSIM/LPIPS
w/o LRD	25.12/0.909/0.281	20.69/0.827/0.503	20.71/0.883/0.384	21.27/0.766/0.418	17.76/0.459/0.494	21.11/0.769/0.416
w/ TV	25.33/0.909/0.285	20.75/0.827/0.503	20.74/0.883/0.387	20.52/0.764/0.424	17.94/0.518/0.478	21.06/0.780/0.415
w/ LRD	30.03/0.918/0.274	29.27/0.879/0.345	30.00/0.900/0.380	23.82/0.782/0.451	18.26/0.561/0.439	26.28/0.808/0.379
LRD+TV	30.03/0.919/0.274	29.27/0.849/0.345	30.01/0.900/0.379	23.82/0.779/0.451	18.15/0.500/0.464	26.27/0.789/0.383

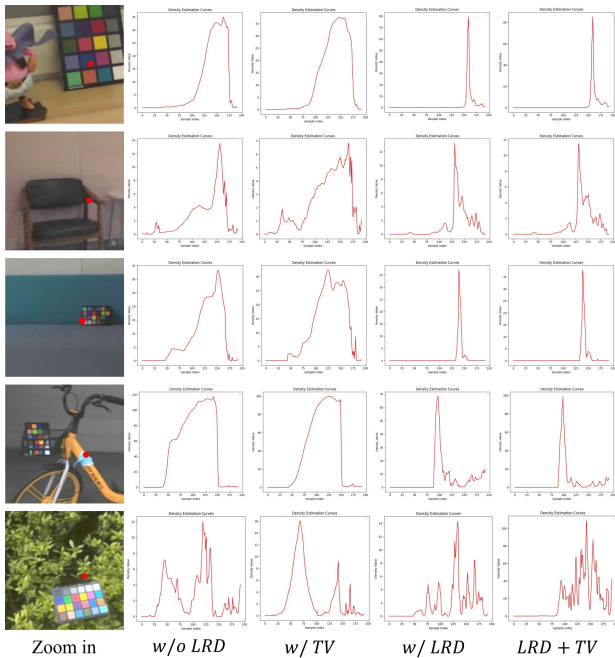


Figure 5. Density distribution of sampling points along the camera ray, with zoomed-in image pixels for better observation. “w/o” and “w/” denote the absence and presence, respectively. “TV” refers to total variation loss [13].

correct object density estimation, leading to broader density distributions. While TV loss provides some denoising effects, LRD achieves superior results with narrower distributions. The combination of LRD and TV loss does not yield additional improvements, due to their overlapping roles. Quantitative results in Table 3 confirm that LRD significantly improves performance, whereas TV loss provides limited benefit due to detail loss during denoising. In complex scenes like “bike” and “shrub,” LRD’s gains are relatively modest, as these scenes require more complex illuminance transition modeling, which can be addressed by increasing sampling points.

## 5. Conclusions

In this paper, we propose RoSe, an unsupervised approach for robust low-light scene restoration. Unlike conventional Retinex-based decomposition and enhancement, we reformulate low-light restoration as an illuminance transition estimation problem and conceptualize this as a specialized neural radiance field. This leads to a concise dual-branch network consisting of a viewer-centered normal-light scene representation branch and a world-centered illuminance transition estimation branch, with a low-rank denoising module integrated to eliminate artifacts and improve structural integrity. Extensive experiments demonstrate that RoSe outperforms current state-of-the-art methods in both visual quality and multi-view consistency.

RoSe currently relies on the Lambertian assumption [29], and explicit modeling of specular reflection will be explored in the future to improve realism. Moreover, RoSe can also be integrated into efficient NeRF variants [3, 21] to accelerate training. However, this efficiency gain currently comes at the cost of quality degradation. Addressing this trade-off – as well as enabling generalization across scenes without per-scene training – offers an important direction for future research.

## Acknowledgments

The work described in this paper was supported, in part, by the Innovation and Technology Fund (Projects: ITP/052/23TP & ITP/004/24TP) and by the Research Institute for Intelligent Wearable Systems (Grant: CD95/P0049355) and the Research Centre of Textiles for Future Fashion (Grants: BDVH/P0051330 & BBFL/P0052601) of The Hong Kong Polytechnic University. It was also supported by the National Natural Science Foundation of China (Grant No. 62202241), Jiangsu Province Natural Science Foundation for Young Scholars (Grant No. BK20210586), NUPTSF (Grant No. NY221018), and Double-Innovation Doctor Program under Grant JSSCBS20220657.

## References

- [1] Tim Brooks, Ben Mildenhall, Tianfan Xue, Jiawen Chen, Dillon Sharlet, and Jonathan T Barron. Unprocessing images for learned raw denoising. In *Proceedings of the IEEE/CVF conference on computer vision and pattern recognition*, pages 11036–11045, 2019. 5
- [2] Yuanhao Cai, Hao Bian, Jing Lin, Haoqian Wang, Radu Timofte, and Yulun Zhang. Retinexformer: One-stage retinex-based transformer for low-light image enhancement. In *Proceedings of the IEEE/CVF International Conference on Computer Vision*, pages 12504–12513, 2023. 3, 6, 7
- [3] Anpei Chen, Zexiang Xu, Andreas Geiger, Jingyi Yu, and Hao Su. Tensorf: Tensorial radiance fields. In *European conference on computer vision*, pages 333–350. Springer, 2022. 8
- [4] Ziteng Cui, Kunchang Li, Lin Gu, Shenghan Su, Peng Gao, Zhengkai Jiang, Yu Qiao, and Tatsuya Harada. You only need 90k parameters to adapt light: a light weight transformer for image enhancement and exposure correction. *arXiv preprint arXiv:2205.14871*, 2022. 1, 2, 6, 7
- [5] Ziteng Cui, Lin Gu, Xiao Sun, Xianzheng Ma, Yu Qiao, and Tatsuya Harada. Aleth-nerf: Illumination adaptive nerf with concealing field assumption. In *Proceedings of the AAAI Conference on Artificial Intelligence*, pages 1435–1444, 2024. 1, 2, 5, 6, 7
- [6] Sara Fridovich-Keil, Alex Yu, Matthew Tancik, Qinhong Chen, Benjamin Recht, and Angjoo Kanazawa. Plenoxels: Radiance fields without neural networks. In *Proceedings of the IEEE/CVF conference on computer vision and pattern recognition*, pages 5501–5510, 2022. 2
- [7] Stephan J Garbin, Marek Kowalski, Matthew Johnson, Jamie Shotton, and Julien Valentin. Fastnerf: High-fidelity neural rendering at 200fps. In *Proceedings of the IEEE/CVF international conference on computer vision*, pages 14346–14355, 2021. 2
- [8] Chunle Guo, Chongyi Li, Jichang Guo, Chen Change Loy, Junhui Hou, Sam Kwong, and Runmin Cong. Zero-reference deep curve estimation for low-light image enhancement. In *Proceedings of the IEEE/CVF conference on computer vision and pattern recognition*, pages 1780–1789, 2020. 1, 2, 3, 6, 7
- [9] Xiaojie Guo, Yu Li, and Haibin Ling. Lime: Low-light image enhancement via illumination map estimation. *IEEE Transactions on image processing*, 26(2):982–993, 2016. 6, 7
- [10] Ajay Jain, Matthew Tancik, and Pieter Abbeel. Putting nerf on a diet: Semantically consistent few-shot view synthesis. In *Proceedings of the IEEE/CVF International Conference on Computer Vision*, pages 5885–5894, 2021. 2
- [11] Yifan Jiang, Xinyu Gong, Ding Liu, Yu Cheng, Chen Fang, Xiaohui Shen, Jianchao Yang, Pan Zhou, and Zhangyang Wang. Enlighthan: Deep light enhancement without paired supervision. *IEEE transactions on image processing*, 30:2340–2349, 2021. 2
- [12] Injae Kim, Minhyuk Choi, and Hyunwoo J Kim. Up-nerf: Unconstrained pose prior-free neural radiance field. *Advances in Neural Information Processing Systems*, 36, 2024. 2
- [13] Ron Kimmel, Michael Elad, Doron Shaked, Renato Keshet, and Irwin Sobel. A variational framework for retinex. *International Journal of computer vision*, 52:7–23, 2003. 7, 8
- [14] Chongyi Li, Chunle Guo, and Chen Change Loy. Learning to enhance low-light image via zero-reference deep curve estimation. *IEEE transactions on pattern analysis and machine intelligence*, 44(8):4225–4238, 2021. 3
- [15] Risheng Liu, Long Ma, Jiaao Zhang, Xin Fan, and Zhongxuan Luo. Retinex-inspired unrolling with cooperative prior architecture search for low-light image enhancement. In *Proceedings of the IEEE/CVF conference on computer vision and pattern recognition*, pages 10561–10570, 2021. 1, 2, 3, 6, 7
- [16] Feifan Lv, Feng Lu, Jianhua Wu, and Chongsoon Lim. Mblen: Low-light image/video enhancement using cnns. In *Bmvc*, page 4. Northumbria University, 2018. 3, 6
- [17] Long Ma, Tengyu Ma, Risheng Liu, Xin Fan, and Zhongxuan Luo. Toward fast, flexible, and robust low-light image enhancement. In *Proceedings of the IEEE/CVF conference on computer vision and pattern recognition*, pages 5637–5646, 2022. 1, 3, 6, 7
- [18] Ricardo Martin-Brualla, Noha Radwan, Mehdi SM Sajjadi, Jonathan T Barron, Alexey Dosovitskiy, and Daniel Duckworth. Nerf in the wild: Neural radiance fields for unconstrained photo collections. In *Proceedings of the IEEE/CVF conference on computer vision and pattern recognition*, pages 7210–7219, 2021. 2
- [19] Ben Mildenhall, Pratul P Srinivasan, Matthew Tancik, Jonathan T Barron, Ravi Ramamoorthi, and Ren Ng. Nerf: Representing scenes as neural radiance fields for view synthesis. *Communications of the ACM*, 65(1):99–106, 2021. 1, 2, 5, 6
- [20] Ben Mildenhall, Peter Hedman, Ricardo Martin-Brualla, Pratul P Srinivasan, and Jonathan T Barron. Nerf in the dark: High dynamic range view synthesis from noisy raw images. In *Proceedings of the IEEE/CVF conference on computer vision and pattern recognition*, pages 16190–16199, 2022. 2
- [21] Thomas Müller, Alex Evans, Christoph Schied, and Alexander Keller. Instant neural graphics primitives with a multiresolution hash encoding. *ACM transactions on graphics (TOG)*, 41(4):1–15, 2022. 8
- [22] Michael Niemeyer, Jonathan T Barron, Ben Mildenhall, Mehdi SM Sajjadi, Andreas Geiger, and Noha Radwan. Reg-nerf: Regularizing neural radiance fields for view synthesis from sparse inputs. In *Proceedings of the IEEE/CVF Conference on Computer Vision and Pattern Recognition*, pages 5480–5490, 2022. 2
- [23] Zia-ur Rahman, Daniel J Jobson, and Glenn A Woodell. Retinex processing for automatic image enhancement. *Journal of Electronic imaging*, 13(1):100–110, 2004. 2, 3
- [24] Christian Reiser, Songyou Peng, Yiyi Liao, and Andreas Geiger. Kilonerf: Speeding up neural radiance fields with thousands of tiny mlps. In *Proceedings of the IEEE/CVF international conference on computer vision*, pages 14335–14345, 2021. 2

- [25] Weining Ren, Zihan Zhu, Boyang Sun, Jiaqi Chen, Marc Pollefeys, and Songyou Peng. Nerf on-the-go: Exploiting uncertainty for distractor-free nerfs in the wild. In *Proceedings of the IEEE/CVF Conference on Computer Vision and Pattern Recognition*, pages 8931–8940, 2024. 2
- [26] Viktor Rudnev, Mohamed Elgharib, William Smith, Lingjie Liu, Vladislav Golyanik, and Christian Theobalt. Nerf for outdoor scene relighting. In *European Conference on Computer Vision*, pages 615–631. Springer, 2022. 2
- [27] Sara Sabour, Suhani Vora, Daniel Duckworth, Ivan Krasin, David J Fleet, and Andrea Tagliasacchi. Robustnerf: Ignoring distractors with robust losses. In *Proceedings of the IEEE/CVF Conference on Computer Vision and Pattern Recognition*, pages 20626–20636, 2023. 2
- [28] Aashish Sharma and Robby T Tan. Nighttime visibility enhancement by increasing the dynamic range and suppression of light effects. In *Proceedings of the IEEE/CVF Conference on Computer Vision and Pattern Recognition*, pages 11977–11986, 2021. 2
- [29] JA Smith, Tzeu Lie Lin, KJ Ranson, et al. The lambertian assumption and landsat data. *Photogrammetric Engineering and Remote Sensing*, 46(9):1183–1189, 1980. 8
- [30] Nagabhushan Somraj and Rajiv Soundararajan. Vip-nerf: Visibility prior for sparse input neural radiance fields. In *ACM SIGGRAPH 2023 Conference Proceedings*, pages 1–11, 2023. 2
- [31] Yunkai Tang, Chengxuan Zhu, Renjie Wan, Chao Xu, and Boxin Shi. Neural underwater scene representation. In *Proceedings of the IEEE/CVF Conference on Computer Vision and Pattern Recognition*, pages 11780–11789, 2024. 2
- [32] Marco Toschi, Riccardo De Matteo, Riccardo Spezialetti, Daniele De Gregorio, Luigi Di Stefano, and Samuele Salti. Relight my nerf: A dataset for novel view synthesis and relighting of real world objects. In *Proceedings of the IEEE/CVF Conference on Computer Vision and Pattern Recognition*, pages 20762–20772, 2023. 2
- [33] Ashish Vaswani, Noam Shazeer, Niki Parmar, Jakob Uszkoreit, Llion Jones, Aidan N Gomez, Łukasz Kaiser, and Illia Polosukhin. Attention is all you need. *Advances in neural information processing systems*, 30, 2017. 5
- [34] Haoyuan Wang, Xiaogang Xu, Ke Xu, and Rynson WH Lau. Lighting up nerf via unsupervised decomposition and enhancement. In *Proceedings of the IEEE/CVF International Conference on Computer Vision*, pages 12632–12641, 2023. 1, 2, 6, 7
- [35] Chen Wei, Wenjing Wang, Wenhan Yang, and Jiaying Liu. Deep retinex decomposition for low-light enhancement. In *British Machine Vision Conference 2018, BMVC 2018, Newcastle, UK, September 3-6, 2018*, page 155. BMVA Press, 2018. 3, 6, 7
- [36] Wenhui Wu, Jian Weng, Pingping Zhang, Xu Wang, Wenhan Yang, and Jianmin Jiang. Uretinex-net: Retinex-based deep unfolding network for low-light image enhancement. In *Proceedings of the IEEE/CVF conference on computer vision and pattern recognition*, pages 5901–5910, 2022. 2, 3
- [37] Xiaogang Xu, Ruixing Wang, Chi-Wing Fu, and Jiaya Jia. Snr-aware low-light image enhancement. In *Proceedings of the IEEE/CVF conference on computer vision and pattern recognition*, pages 17714–17724, 2022. 2
- [38] Yingyan Xu, Gaspard Zoss, Prashanth Chandran, Markus Gross, Derek Bradley, and Paulo Gotardo. Renerf: Relightable neural radiance fields with nearfield lighting. In *Proceedings of the IEEE/CVF International Conference on Computer Vision*, pages 22581–22591, 2023. 2
- [39] Shuzhou Yang, Moxuan Ding, Yanmin Wu, Zihan Li, and Jian Zhang. Implicit neural representation for cooperative low-light image enhancement. In *Proceedings of the IEEE/CVF international conference on computer vision*, pages 12918–12927, 2023. 2
- [40] Wenhan Yang, Wenjing Wang, Haofeng Huang, Shiqi Wang, and Jiaying Liu. Sparse gradient regularized deep retinex network for robust low-light image enhancement. *IEEE Transactions on Image Processing*, 30:2072–2086, 2021. 2
- [41] Xunpeng Yi, Han Xu, Hao Zhang, Linfeng Tang, and Jiayi Ma. Diff-retinex: Rethinking low-light image enhancement with a generative diffusion model. In *Proceedings of the IEEE/CVF International Conference on Computer Vision*, pages 12302–12311, 2023. 3
- [42] Alex Yu, Vickie Ye, Matthew Tancik, and Angjoo Kanazawa. pixelnerf: Neural radiance fields from one or few images. In *Proceedings of the IEEE/CVF conference on computer vision and pattern recognition*, pages 4578–4587, 2021. 2
- [43] Fan Zhang, Yu Li, Shaodi You, and Ying Fu. Learning temporal consistency for low light video enhancement from single images. In *Proceedings of the IEEE/CVF conference on computer vision and pattern recognition*, pages 4967–4976, 2021. 1, 3, 6, 7
- [44] Qing Zhang, Yongwei Nie, and Wei-Shi Zheng. Dual illumination estimation for robust exposure correction. In *Computer graphics forum*, pages 243–252. Wiley Online Library, 2019. 6, 7
- [45] Tianyi Zhang and Matthew Johnson-Roberson. Beyond nerf underwater: Learning neural reflectance fields for true color correction of marine imagery. *IEEE Robotics and Automation Letters*, 2023. 2
- [46] Xiuming Zhang, Pratul P Srinivasan, Boyang Deng, Paul Debevec, William T Freeman, and Jonathan T Barron. Nerfactor: Neural factorization of shape and reflectance under an unknown illumination. *ACM Transactions on Graphics (ToG)*, 40(6):1–18, 2021. 2
- [47] Anqi Zhu, Lin Zhang, Ying Shen, Yong Ma, Shengjie Zhao, and Yicong Zhou. Zero-shot restoration of underexposed images via robust retinex decomposition. In *2020 IEEE International Conference on Multimedia and Expo (ICME)*, pages 1–6. IEEE, 2020. 3